

# Gold Nanoparticles Supported in Zirconia–Ceria Mesoporous Thin Films: A Highly Active Reusable Heterogeneous Nanocatalyst

Ianina L. Violi,<sup>†</sup> Andrés Zelcer,<sup>\*,†,||</sup> Mariano M. Bruno,<sup>‡,||</sup> Vittorio Luca,<sup>§</sup> and Galo J. A. A. Soler-Illia<sup>†,⊥</sup>

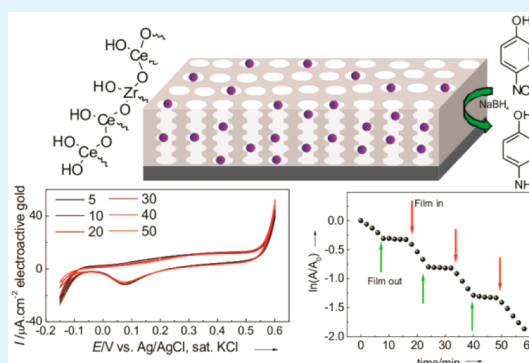
<sup>†</sup>Gerencia Química, Centro Atómico Constituyentes, <sup>‡</sup>Gerencia Física, and <sup>§</sup>Programa Nacional de Gestión de Residuos Radioactivos, Comisión Nacional de Energía Atómica (CAC–CNEA), Av. Gral Paz 1499, San Martín, Buenos Aires, Argentina

<sup>||</sup>ECyT, Universidad Nacional de San Martín, San Martín, Buenos Aires, Argentina

<sup>⊥</sup>DQIAQF, Facultad de Ciencias Exactas y Naturales, Universidad de Buenos Aires, Buenos Aires, Argentina

## Supporting Information

**ABSTRACT:** Gold nanoparticles (NP) trapped in the mesopores of mixed zirconia–ceria thin films are prepared in a straightforward and reproducible way. The films exhibit enhanced stability and excellent catalytic activity in nitro-group reduction by borohydride and electrocatalytic activity in CO and ethanol oxidation and oxygen reduction.



**KEYWORDS:** mesoporous materials, thin films, gold catalysis, zirconia ceria, electrocatalysis

## INTRODUCTION

Gold has gained increased attention as catalyst<sup>1–3</sup> since the unexpected finding of its high activity.<sup>4</sup> In particular, its high activity in selective oxidations,<sup>5</sup> hydrogenations,<sup>6</sup> and the water–gas shift (WGS) reaction have relevant ramifications as far as their applications are concerned. Gold catalysis can be performed either homogeneously with molecular complexes or heterogeneously using Au nanoparticles (NPs).<sup>7</sup> Catalysis by Au NPs can be performed using suspended colloidal NPs or supported NPs. Different synthesis routes permit the preparation of colloidal Au NPs with a very precise control of shape, size, geometry, and crystalline arrangement. This exquisite tuning of NPs properties makes them an ideal platform for the systematic study of the influence of each of these parameters in the catalytic activity. However, colloidal NPs show many limitations when considered for actual applications. In particular, the reusability<sup>8</sup> of colloidal suspensions is very limited due to activity loss and difficult recovery. Suspended metallic NPs must have a capping agent that lowers the free energy of the surface, preventing aggregation and flocculation. After prolonged use in catalysis, this capping layer is eventually lost,<sup>9</sup> leading to aggregation and a marked decrease of activity. Furthermore, if the catalyst is to be reused, separation by time-consuming centrifugation is required. This leads not only to increased costs and times but also to the risk of undesired presence of the catalyst in the reaction product.

In contrast, supported NPs are complex systems, more difficult to control. The resulting heterogeneous NPs properties and environments make them less attractive as model systems for the systematic studies of fundamental processes in catalysis. Nevertheless, supported catalysts are simpler to separate and recover from the reaction mixture, enhancing the reusability if the activity is maintained. In addition, the support might be involved in the catalysis process, either promoting or modulating the activity of the NP. In some cases the proper choice of the support material can be as relevant as the choice of the catalyst. The NP–support interface plays an active role in many catalytic systems on which the support takes an active part in the catalytic cycle or enhances NP stability.<sup>10,11</sup> In particular, mesoporous systems with high surface area and accessibility represent an excellent platform for catalysis<sup>12</sup> and an ultimate example of integrated nanocatalysts in which the active nanophases are incorporated into support matrices that may contribute to overall catalytic processes.<sup>13</sup> Indeed, mesopore curvature effects might assist reaction kinetics, as was suggested to account for the high activity of metallic NP embedded in mesoporous materials. For example, the high activity of metallic NPs in mesoporous silica<sup>14</sup> was attributed to the particular geometry of silanol groups on a concave surface. Recently, it was observed that WGS catalytic activity was higher

**Received:** September 26, 2014

**Accepted:** December 18, 2014

**Published:** December 18, 2014

for NPs embedded in mesoporous ceria compared to those deposited on a flat surface. The lowering of the activation energy was attributed to the concave topology of the CeO<sub>2</sub> internal walls.<sup>15</sup>

Although small particulate materials are often used as catalysts and catalyst supports,<sup>16–18</sup> small mesoporous particles require time-consuming procedures to separate and reuse, especially when employed in fine chemical synthesis. Centrifugation and membrane filtration are limited to small scales. Filtration through adsorbents like Celite is a common practice, but the catalyst is not recovered in its initial state<sup>8</sup> but is mixed with the filtration media.<sup>19</sup> Moreover, the homogeneous loading of monodisperse metallic NP into mesoporous materials is a critical aspect to reproducibly obtain useful catalysts.<sup>20</sup> Catalytic NPs are often poorly included and dispersed in mesoporous particles due to diffusion and adsorption kinetics in the mesopores.

Since mesoporous thin films (MTF) can be deposited onto many substrates, including conductive surfaces, this particular system can be employed in electrochemical reactions, flow chemistry, and lab-on-a-chip systems. Even if the electrocatalytic properties of AuNPs have been well-documented,<sup>21,22</sup> most work has been performed using small area systems of complex preparation, inappropriate for applications.

In the present article, we report the synthesis and catalytic properties of Au NPs deposited within the pores of Zr<sub>1-x</sub>Ce<sub>x</sub>O<sub>2</sub> (0 ≤ x ≤ 0.5) MTF. This choice of support material and processing method leads to highly active and recoverable<sup>8</sup> catalysts with remarkable stability in alkaline conditions. In particular, we address the issues of reusability and flexibility of application of this nanocomposite material that can be used for heterogeneous catalysis or even electrocatalysis. The materials are highly active in a variety of reactions and can be completely and easily recovered without requiring centrifugation or filtration, resulting in a versatile catalytic platform.

## EXPERIMENTAL SECTION

**Materials.** 4-Nitrophenol (4NIP), Zr(PrO)<sub>4</sub> (70% in propanol), CeCl<sub>3</sub>·7H<sub>2</sub>O, acetylacetone (acac), Pluronic F127, and HAuCl<sub>4</sub> were purchased from Sigma-Aldrich. KOH, NaOH, absolute ethanol, and HCl were purchased from Merck. NaBH<sub>4</sub> was obtained from Riedel-de Haën. All reagents were used as received. Silicon, bare glass, and indium-doped tin oxide (ITO, Deta Tech) coated glass were used as substrates for thin film deposition. Water (resistivity 18 MΩ·cm) was obtained from a Millipore system.

**Methods.** *Thin Film Preparation.* Initial solutions were prepared using Zr(PrO)<sub>4</sub> and CeCl<sub>3</sub>·7H<sub>2</sub>O as the inorganic sources, acetylacetone (acac) as stabilizing agent, and Pluronic F127 as pore template. The final Zr(PrO)<sub>4</sub>:CeCl<sub>3</sub>:EtOH:H<sub>2</sub>O:acac:HCl:F127 molar ratios were 1-x:x:40:20:1-x:1:0.005, where x was varied between 0.1 and 0.5.

For the preparation of MTFs, initial solutions were dip-coated onto silicon and ITO at withdrawal speeds of 1.0 mm·s<sup>-1</sup> or onto soda-lime glass using withdrawal speeds between 0.5 and 4.0 mm·s<sup>-1</sup>. After film deposition, films were heated at 200 °C for 30 min on a still-air oven. The films were finally calcined at 350 °C for 2 h with a heating ramp of 1 °C min<sup>-1</sup>.

*Gold Nanoparticles Preparation.* Gold nanoparticles (Au NPs) were incorporated to the MTFs through an in situ adsorption–reduction method.<sup>23</sup> Briefly, films were introduced during 1 min in 1 mM HAuCl<sub>4</sub> adjusted at pH = 4 with NaOH 0.1M, then copiously rinsed with Millipore water and dried at room temperature under air current. After that, the films were introduced for 1 min in 10 mM NaBH<sub>4</sub> to reduce the adsorbed gold species and finally rinsed and dried again using the same procedure. This procedure represents one

adsorption–reduction cycle, and it can be repeated to obtain higher gold loading.

*Materials Characterization.* Morphology of the films was studied using transmission electron microscopy (TEM Phillips EM 301 CMA, Facultad de Ciencias Exactas y Naturales, UBA) and field emission scanning electron microscopy (FESEM, Carl-Zeiss SUPRA 40, CMA, Facultad de Ciencias Exactas y Naturales, UBA). Au NPs growth was monitored using an HP8453 spectrophotometer. Gold was quantified by energy-dispersive X-ray spectroscopy (EDS) coupled to FESEM and by X-ray reflectometry (XRR, D10A-XRD2 line at Laboratório Nacional de Luz Síncrotron, Brazil) as previously reported.<sup>24</sup> Briefly, the critical angle, which depends on the average electronic density of the film, is measured before and after Au loading. The changes in this value are directly related to the amount of Au deposited inside the pores. Au NP size distribution was determined, measuring between 40 and 70 particles in TEM and FESEM images. Porosity and pore dimensions were determined by environmental ellipsoporosimetry (EEP, SOPRA GESSA). Pore arrangement and interplanar distances were measured using small angle X-ray scattering and X-ray reflectometry (SAXS, Laboratório Nacional de Luz Síncrotron, Brazil). Crystalline phases were characterized by grazing incidence X-ray diffraction (GIXRD, PANalytical Empyrean in grazing incidence configuration).

*4NIP Reduction Kinetics.* 4NIP reduction kinetics by NaBH<sub>4</sub> was followed measuring the absorbance (Hewlett-Packard 8453) at λ = 400 nm of a 4NIP solution in contact with the catalyst within 2 min intervals. Reaction solution was prepared mixing 2.5 g of Millipore water + 10 μL of 0.01 M 4-NIP + 100 μL of 0.5 M NaBH<sub>4</sub>. A piece of ~1 cm<sup>2</sup> glass-supported catalyst was introduced to start the reaction. In the leaching tests, the glass substrate supporting the mesoporous film was successively removed and reintroduced into the reaction media to evaluate the reaction kinetics in absence and presence of the supported catalyst.

*Electrochemical Measurements.* Cyclic voltammetry (CV) measurements were performed on an Autolab PGSTAT30N, using a jacked electrochemical cell at 25 °C. Ag/AgCl (sat. KCl) electrode and a Pt wire were used as reference (RE) and counter electrodes (CE), respectively. The working electrode (WE) consisted of a piece of ITO coated with film and loaded with Au NPs. The WE was connected electrically through a small section of the ITO substrate free of mesoporous film using a gold wire. All of the solutions were prepared using Millipore water. KOH solutions were deoxygenated by bubbling with nitrogen gas for at least 30 min. Before electrocatalytic CO oxidation measurements, the KOH solution was saturated with CO for 30 min. The electroactive surface area of gold nanoparticles was determined assuming 400 μC cm<sup>-2</sup> for the reduction of a monolayer of gold oxide at a polycrystalline surface.<sup>25</sup>

The turnover frequency (TOF) for CO oxidation was calculated by chronoamperometric measurements.<sup>26–28</sup> The catalysts were immersed on a CO-saturated 0.5 M KOH solution, and the potential was fixed at 0.00 V versus Ag/AgCl. The steady-state current density was measured at 80 s.

## RESULTS AND DISCUSSION

**Support Design and Characterization.** To obtain NP-mesoporous films with high activity and enhanced stability, we prepared Au NPs inside the pores of Zr<sub>1-x</sub>Ce<sub>x</sub>O<sub>2</sub> (0 ≤ x ≤ 0.5) MTFs (ZrCe MTF). Zirconia-ceria based oxides are the matrix of choice for several reasons: (a) there is evidence of a stabilizing effect of ZrO<sub>2</sub> toward Au NP,<sup>29</sup> (b) there is a positive support effect of Ce containing materials for redox catalysis,<sup>30,31</sup> and (c) Au catalysis in solution usually requires alkaline conditions,<sup>21</sup> and this family of materials withstands harsh alkaline conditions without deterioration.<sup>32</sup> Other accessible mesoporous materials like SiO<sub>2</sub> and Al<sub>2</sub>O<sub>3</sub> readily dissolve in alkaline solutions, and are inadequate for Au NP-based catalysis. The films were deposited by dip-coating a sol prepared using zirconium *n*-propoxide and cerium chloride as

metal oxide precursors, the commercial surfactant Pluronic F127 as a template, and acetylacetonone and hydrochloric acid as reactivity moderators.<sup>32</sup> The relative amount of metals can be varied from  $x = 0$  to  $x = 0.5$  yielding optical-quality films composed of homogeneous zirconia–ceria solid solutions. No segregation of zirconium- and cerium-rich phases was observed under electronic microscopes (Figure 1A,B) or GIDRX

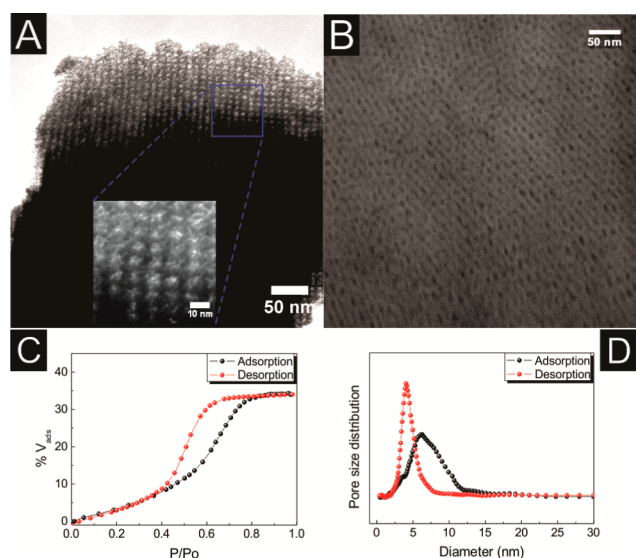


**Figure 1.** (A) TEM images of a  $Zr_{0.5}Ce_{0.5}O_2$  thin film. (B) Top-view FESEM image of a  $Zr_{0.9}Ce_{0.1}O_2$  thin film. (C) Accessible volume as a function of the relative water pressure. (D) Pore size distribution. Both (C) and (D) determined by environmental ellipsoriposimetry.

(Supporting Information, Figures S1 and S2). The preparation is straightforward, applicable to large surfaces, and requires little time. Glass, silicon, and indium tin oxide (ITO) coated glass were used as substrates. The thickness of the films was controlled varying the withdrawal speed. Thicknesses between 50 and 140 nm were obtained varying the withdrawal speed between 0.5 and 4.0  $\text{mm}\cdot\text{s}^{-1}$ .

EEP and SAXS studies show that the films have a high accessible ordered porosity of ca. 30% (Figure 1C). Low incidence angle SAXS ( $3^\circ$ ) show a diffraction pattern compatible with a distorted  $Im\bar{3}m$  mesopore arrangement. The measured [110] interplanar distances are of 13.5 nm (Supporting Information, Figure S3) with almost no variation with film composition. The pore characteristics were measured using EEP. The existence of a strong type IV hysteresis with an H2 loop is consistent with a network of pores interconnected with necks of smaller dimensions. A 6 nm average pore diameter and 4 nm neck was measured using the adsorption and desorption branches of the isotherms (Figure 1D). The pore sizes and arrangement are the same for all compositions tested. GIXRD experiments show that the films present homogeneous nanocrystalline inorganic walls (Supporting Information, Figures S1 and S2), with an atomic-scale mixing of Zr and Ce centers.

**Au NP Catalyst Deposition.** Au NPs having mean diameters of  $5 \pm 1$  nm were deposited within the mesopores by impregnation–reduction cycles (Figure 2A,B).<sup>23</sup> Gold species are first adsorbed on the mesoporous oxide by immersion on a  $\text{HAuCl}_4$  solution (60 s), followed by a brief rinse to remove nonadsorbed species and reduction by immersion on a  $\text{NaBH}_4$  solution (60 s). The amount of gold adsorbed in this procedure

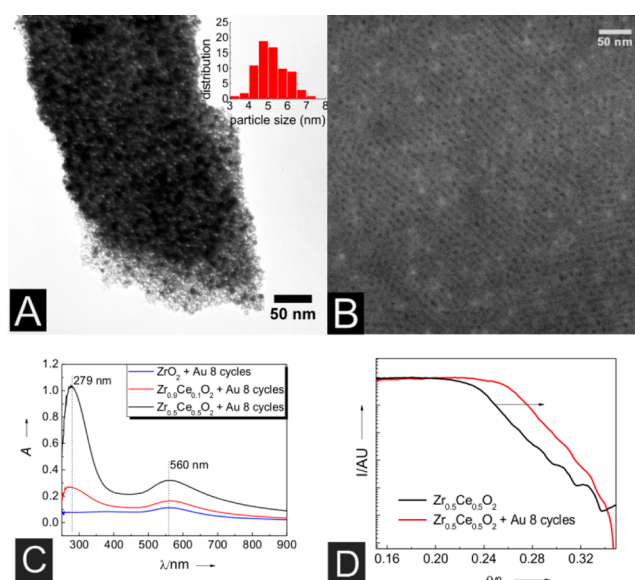


**Figure 2.** (A) TEM image of a  $Zr_{0.5}Ce_{0.5}O_2$  thin film with deposited AuNPs (inset Au particle size distribution). (B) FESEM images of  $Zr_{0.9}Ce_{0.1}O_2$  thin film with deposited AuNPs through eight adsorption–reduction cycles. (C) UV–vis spectra of different  $Zr_{1-x}Ce_xO_2$  MTFs deposited onto soda-lime glass, after eight adsorption–reduction cycles. (D) Normalized X-ray reflectivity of  $Zr_{0.5}Ce_{0.5}O_2$  MTF without gold (0 cycles) and after eight adsorption–reduction cycles.

is controlled by the relative Zr/Ce atomic ratio of the pore walls (Table 1). The different points of zero charge (PZCs) of

**Table 1. Gold Load for Different Zr/Ce Atomic Ratios and Impregnation–Reduction Cycles**

$x^a$	cycles	Au, $\text{g}\cdot\text{cm}^{-3}$
0	0	
	8	0.09
	12	0.29
0.3	0	
	6	0.23
0.5	12	0.76
	0	
	4	0.37
	6	0.66
	8	0.78
	10	0.79

<sup>a</sup>The  $x$  value represents the Zr to total metal content of the mesoporous support (Zr + Ce).

both metal oxides<sup>33</sup> allow modulating the material surface charge and thus the amount of Au(III) species adsorbed. Gold loading can be further controlled by varying the number of adsorption–reduction cycles. Films turn pink-violet after the first cycle, and after eight cycles they are completely purple. This color is originated in a strong light absorption due to the Au NP plasmon resonance. Transmission UV–vis analysis of the films shows indeed a band centered on 560 nm attributed to the Au NPs (Figure 2C). The band at 279 nm corresponds to a charge-transfer transition between oxygen and Ce(IV) centers typical of cerium in an oxide environment,<sup>34</sup> and increases accordingly with Ce content of the films.

The measured size of the NPs is the same for all wall compositions and number of adsorption–reduction cycles. It seems that under these conditions NP growth is considerably faster than seed formation and this leads to uniformly sized NPs. Nevertheless, it is possible that small isolated atomic clusters exist sorbed to the oxide surface. Comparison of the EEP sorption isotherms before and after infiltration with Au NPs (Supporting Information, Figure S4) shows that the material retains a high accessible porous volume. Nevertheless, there is a decrease caused by the inclusion of the nanoparticles into the pores.

Using this method the Au/M ( $M = \text{Zr} + \text{Ce}$ ) atomic ratio can be tuned from 2.5% to 18% and Au loadings up to  $0.79 \text{ g of Au cm}^{-3}$  were achieved. Since the reduced gold species are initially adsorbed on the mesopore walls, the NP deposition method has several advantages over traditional methods: (a) the Au NPs remain trapped inside the mesopores (Figure 2B), (b) the metal-oxide interface, which is known to be relevant to many catalytic processes,<sup>35–38</sup> is inherited from the adsorbed precursor, (c) no separate NP preparation is required, resulting in faster and greener preparations, since no organic solvents or toxic stabilizers are employed, and (d) the nanoparticle surface is free from strongly bound capping agents. Since the metal NP maximum size is limited by the pore dimensions, using a different template for mesopore formation would lead to other size-limited NP–mesoporous substrate systems. This strategy can be extended to other support-dictated sized NPs, as has been reported in mesoporous materials with controlled plasmonic properties<sup>23,39</sup>

This ship-in-a-bottle strategy employed to create the NPs by in situ reduction inside the mesopores relies in an adequate control of the pore surface charge.<sup>40</sup> The pH during adsorption must be tuned according to mesoporous wall PZC and metal precursor acid–base behavior to provide an adequate degree of precursor adsorption. Judicious selection of mesoporous material and sorption conditions would therefore allow for tuning of the NP loading. The size could be tuned by using a different surfactant as a mesopore template. The benefits and drawbacks of the present NP deposition method can be assessed through comparison with alternate methods, like capillary inclusion<sup>20</sup> and NP encapsulation.<sup>41</sup> These latter methods allow for a great control over NP properties at the expense of separate NP preparation. On the other hand impregnation–reduction has much lower risk of inhomogeneous loading and external deposition of NPs and is simpler since it does not require separate NPs preparation procedures or capping agent removal. Furthermore, the NP deposition is independent of support preparation, allowing for arbitrary thermal treatments during the preparation of the matrix. The confinement of NP growth and the very fast, out-of-equilibrium reduction step yield quite monodisperse Au NP, avoiding issues present in similar methods employing thermal activation of the catalyst.<sup>41</sup>

**Catalysis Measurements.** The activity and stability of the supported Au NP was studied using model reactions. As an example of reduction, we tested the behavior of the ZrCe MTF supported NPs in the reaction of 4-nitrophenol (4NIP) with  $\text{NaBH}_4$ . This reaction has been well-studied and serves as a benchmark for metal NP catalysis.<sup>42–44</sup>

**Chemical Catalysis: 4NIP Reduction.** The reaction of 4NIP with  $\text{NaBH}_4$  was performed immersing  $\sim 1 \text{ cm}^2$  pieces of glass covered with Au NP-loaded mesoporous films (ca.  $1 \text{ mg of film}$ ) in stirred solutions containing the reactants (Figure 3).

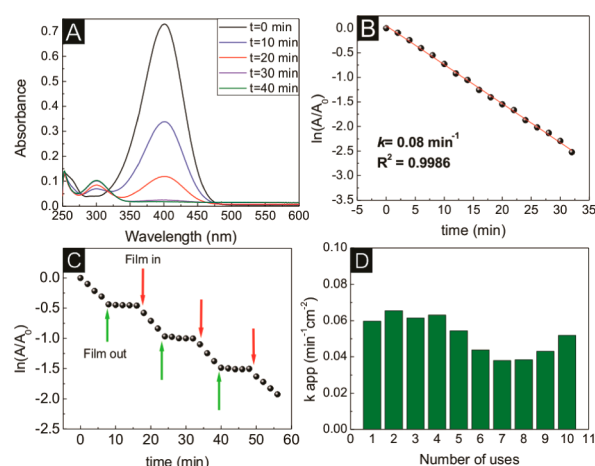


**Figure 3.** 4-Nitrophenol reduction catalysis. (A) Spectra as a function of time. (B) Fit to first-order kinetics. (C) Leaching test: green arrows indicate film withdrawal, and red arrows indicate film reintroduction. (D) Catalyst reutilization.  $x = 0.5$ , 4.0% atomic Au/(Zr + Ce).

These reaction conditions are normally used to measure activity in dispersed catalysts, and thus provide a valid point of activity comparison. Nevertheless, it should be kept in mind that these conditions are suboptimal for a film-supported catalyst since reactant diffusion from solution to support can slow the reaction kinetics. The reaction proceeds immediately after the introduction of the films in the reaction media. In contrast to what is observed using unsupported<sup>42</sup> and polymer-encapsulated<sup>43</sup> particles, no induction period was observed. The reaction rate can be modeled according to pseudo first-order kinetics on 4NIP (Figure 3B). The resulting geometric-area normalized apparent rate constants ( $k_{\text{app}}$ ) reach up to  $0.06 \text{ min}^{-1} \text{ cm}^{-2}$ . The activity per Au mol reaches values as high as  $8.5 \times 10^4 \text{ (s}\cdot\text{mol)}^{-1}$ . When comparing Au-atom based constants, the activity is equivalent to that of equally sized free, dispersed Au NPs measured under similar conditions.<sup>42</sup> Since the catalyst is fully supported, the reaction can be readily and completely stopped by withdrawing the film from the solution (Figure 3C). No active species are leached from the film during the catalytic cycle: the reaction stops immediately as the film is withdrawn from the reaction media and resumes when the film is reintroduced. The same behavior was observed for all Zr/Ce ratios. In contrast, in experiments performed using electrostatically adsorbed AuNPs the reaction proceeds even after the substrate is removed, showing that the catalytic NPs detach from the support to the reaction media (see Supporting Information for experimental details). The exact nature of the active catalyst for this reaction is still debated in literature. While some argue that the leaching of small active species<sup>45</sup> takes place in suspended AuNPs, others show evidence that NPs are in fact the active catalysts.<sup>46</sup> Whatever the exact nature of the catalytic species, leaching can be completely ruled out in this case. This fact is important not only for catalyst stability and reusability but also when product purity is taken into account.

The ease of removal of the supported catalyst and the excellent chemical stability of the support and the NPs inside the mesopores make this system a highly recoverable catalyst. We evaluated the reusability and stability of the catalyst using the same sample running many reactions consecutively. The supported nanoparticles show an outstanding stability: even after 10 consecutive uses the supported nanoparticles retain

complete activity, with the final  $k_{app}$  being almost unchanged (see Figure 3D). Since each measurement lasts at least 30 min (see Figure 3B), this treatment corresponds to more than 5 h of exposure to strong alkaline (aqueous  $\text{NaBH}_4$ , pH = 9.6) reaction media without significant degradation of the activity. TEM (Figure 4) and FESEM (Supporting Information, Figure

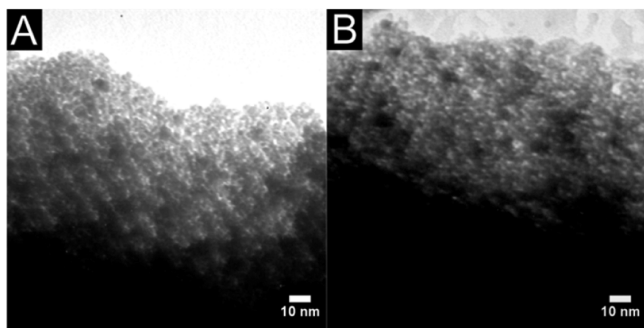


**Figure 4.** TEM images of Au-loaded  $\text{Zr}_{0.5}\text{Ce}_{0.5}\text{O}_2$  thin film before (A) and after (B) catalytic tests.

S5) images show no evident change on the integrity of the MTF matrix and of the NPs after multiple uses, and EDS confirms that the Au/metal ratio is unmodified. Other supports show a rapid decrease in activity due to catalyst mass loss either by dissolution or poor recovery.<sup>47,48</sup> These results show the feasibility of employing this kind of supported catalyst in continuous-flow reactors, particularly in lab-on-a-chip or flow-chemistry applications.

The performance of the catalyst depends on the Au loading and Zr/Ce ratio. In all cases, the reactions could be adjusted to first-order kinetics, and constants could be obtained. When considering the gold-based normalized constants (i.e., per Au atom, see Table 2), the activity becomes smaller for increasing

**Table 2. Au-Normalized First-Order Constants for  $\text{Zr}_{0.5}\text{Ce}_{0.5}\text{O}_2$  Loaded Using Different Number of Adsorption–Reduction Cycles**

cycles	$k_{app}$ ( $\text{s}\cdot\text{Au}_{mol}$ ) <sup>-1</sup>
2	$8.5 \times 10^4$
4	$5.3 \times 10^4$
6	$6.7 \times 10^3$

Au contents. This decrease in specific activity for higher Au loading can be caused by two factors: (a) absorption–reduction cycles can lead to an evolution of highly active small metal atomic clusters into less active NPs, (b) increasing Au NP load might lead to pore clogging, resulting in a hindered reagent or product diffusion through the mesopores. When selecting a system to achieve optimum catalytic activity, either per unit area or Au atom, it should be taken into account that the global activity reflects a synergy of effects that include Au dispersion, surface charge, etc. Indeed, when choosing a catalyst support for a particular reaction, the mixed effects of Au loading, wall composition, and the particular characteristics of that reaction come into play. Although it is tempting to suggest that the reducibility of ceria-rich materials would lead to enhanced activity in certain reactions, many other factors including surface hydroxylation<sup>36,49</sup> and charge<sup>50</sup> also play an important role determining the catalyst activity. Thus, it is necessary to test all these parameters to choose the support–Au loading

combination for each case. Systematic research regarding the performance evaluation of these catalytic systems as a function of Au NP loading, pore size, and wall composition and charge is currently underway.

**Electrochemical Catalysis.** Besides ease of recovery and manipulation, a distinct feature of MTF over powder supports is that they can be readily used in electrochemical reactions. In contrast to previous AuNPs electrochemical studies,<sup>51,52</sup> the  $\text{Zr}_{1-x}\text{Ce}_x\text{O}_2$  MTF-supported Au NPs can be prepared coating large electrode areas, enabling gold-based electrosynthesis in laboratory scale.

The electrocatalytic behavior of the NPs was tested using  $\text{Zr}_{1-x}\text{Ce}_x\text{O}_2$  MTF deposited on ITO-coated glass. Figure 5A

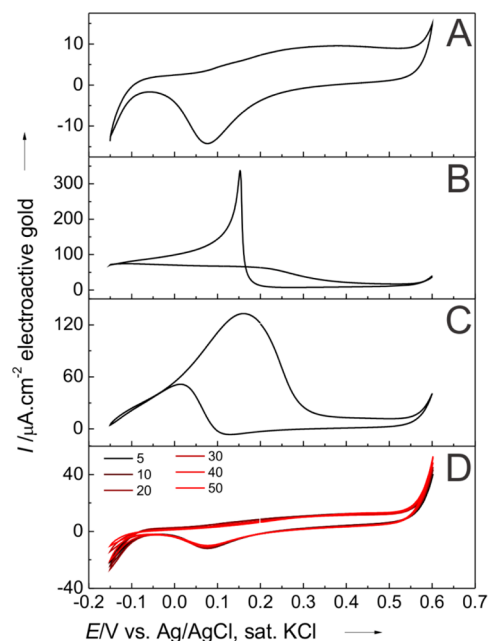


**Figure 5.** CV responses of AuNP/ITO in 0.5 M KOH solution (A) without CO, (B) saturated with CO, and (C) in 0.1 M ethanol solution. (D) Variation of current density in 50 successive scan cycles under continuous  $\text{N}_2$  bubbling. Scan rate:  $5 \text{ mV s}^{-1}$ ; legend indicates scan cycle.

shows the cyclic voltammograms of AuNP@ $\text{Zr}_{0.5}\text{Ce}_{0.5}\text{O}_2$ /ITO in 0.5 M KOH solution. The ZrCe MTF-supported Au NP shows a similar profile to unconfined AuNPs supported onto ITO electrode.<sup>22,51</sup> An oxidation peak is observed at  $\sim 0.37 \text{ V}$  (vs Ag/AgCl) in the anodic sweep, while in the cathodic sweep a reduction peak at  $\sim 0.07 \text{ V}$  is found. These results indicate the formation of gold oxides on the surface of the Au NPs in the anodic scan, whereas the peak in the cathodic scan confirms the reduction of the gold oxides formed.

CO electrooxidation activity is characteristic of Au NPs. Figure 5B shows the cyclic voltammogram of the same system performed in 0.5 M KOH saturated with CO. During the anodic sweep, an oxidation current is observed up to 0.22 V. The anodic current subsequently decreases due to the complete blockage of the electroactive surface by oxide groups. During the cathodic sweep, a negligible current response is observed until an anodic peak, at  $\sim 0.15 \text{ V}$ , can be seen, which is attributed to the sudden onset of the catalytic CO oxidation due to partial reduction of gold oxide groups. The measured turnover frequency (TOF) for this reaction at 0.0 V versus AgCl/Ag is  $1.1 \text{ CO (Au}_{\text{site}} \text{ s})^{-1}$ . To the best of our knowledge,

this is the first time that TOF values of Au-catalyzed CO electrooxidation are reported in literature. The supported AuNPs also exhibit high catalytic activity toward ethanol oxidation and oxygen reduction. Figure 5C shows a cyclic voltammogram in 0.5 M KOH/ethanol 0.1 M. The electro-oxidation response of ethanol on this composite material shows a similar profile to mesoporous gold films.<sup>52</sup> The maximum current value was obtained at 0.16 V (Ag/AgCl), which is attributed to acetate ions as main product of ethanol oxidation.<sup>53</sup> O<sub>2</sub> reduction was studied by saturation of a 0.01 M KOH solution with the gas prior to measuring the CVs. When oxygen is present the cathodic current increases noticeably at lower potentials (Supporting Information, Figure S6). This is attributed to the electrocatalytic activity of gold NPs toward the reduction of oxygen of the electrode to H<sub>2</sub>O<sub>2</sub>.<sup>54</sup>

The extreme robustness of these catalysts allows using the same piece of film to study successively the CV response of the supported Au NPs, the CO electrooxidation, ethanol electro-oxidation, and finally O<sub>2</sub> reduction. Indeed, all the voltammograms shown in Figure 5 were acquired sequentially using the same piece of supported catalyst: after performing each measurement, the film was rinsed, and the electrochemical cell was filled with the solution corresponding to the next experiment. This full set of electrochemical experiments consisted of more than 40 electrochemical cycles. The electrochemical stability of supported NPs was further evaluated subjecting the same sample to CV reaching discharge current at both extreme potentials.

As an extreme test of durability, after these studies the film was rinsed again, and the cell was filled with 0.5 M KOH. After purging with N<sub>2</sub>, 50 cycles were measured from -0.15 to 0.6 V. Figure 5D shows the modification of the electrochemical response of AuNPs during these cycles. Despite the extreme conditions, consisting of 0.5 M KOH and wide potential window, the cathodic peak, which corresponds to the reduction of gold oxides on the surface, retained 83% of its initial integral charge.

## CONCLUSIONS

We have demonstrated that Au NPs supported within the mesopores of mixed ceria-zirconia MTF constitute an integrated highly accessible catalytic system with high activity and an extended stability when used both in catalysis and in electrocatalysis. The ease of manipulation of the systems, in which wall nature, porosity, and Au content can be separately tuned, and the possibility of a complete and straightforward removal and recovery of the catalyst, are very advantageous compared to other supports, being close to those of an "ideal recoverable catalyst".<sup>8</sup> The supported NPs fulfill the high accessibility and stability requirements of flow-chemistry, lab-on-chip, and fuel cell applications.

The adsorption-reduction strategy used for the preparation of the NP in the mesopores provides an accessible alternative for preparing and studying complex systems. A full control of catalyst loading, size, and system composition should be accessible by choosing mesopore size and tuning the catalyst precursor interaction with the support surface. The method could be easily adapted to many support-NP catalyst combinations.

## ASSOCIATED CONTENT

### Supporting Information

SAXS patterns and measured interplanar distances of the reported materials. GIXRD patterns, associated Rietveld refinements, extracted cell volume, and crystallite size. FESEM images and associated Au NP size distribution of supported catalyst before and after use. Experimental details regarding the stability test of electrostatically adsorbed particles. CV showing the oxygen reduction on the supported NPs. Comparative EEP isotherms of mesoporous support before and after deposition of Au NPs. This material is available free of charge via the Internet at <http://pubs.acs.org>.

## AUTHOR INFORMATION

### Corresponding Author

\*E-mail: [zelcer@cnea.gov.ar](mailto:zelcer@cnea.gov.ar).

### Author Contributions

The manuscript was written through contributions of all authors. All authors have given approval to the final version of the manuscript.

### Notes

The authors declare no competing financial interest.

## ACKNOWLEDGMENTS

I.L.V. acknowledges a fellowship from Conicet. A.Z., M.M.B., and G.J.A.A.S.I. are members of Conicet Scientific staff. Funding from Grant Nos. UNSAM SJ/10, PICT 0852, 1848, and 2087 and LNLS Scientific Project 5353 are acknowledged. P.C. Angelomé is acknowledged for critically reading the manuscript. R. Medina is acknowledged for his help during kinetics measurements.

## ABBREVIATIONS

- NP, nanoparticle
- WGS, water-gas shift
- 4NIP, 4-nitrophenol
- MTF, mesoporous thin film
- CV, cyclic voltammetry

## REFERENCES

- (1) Zhang, Y.; Cui, X.; Shi, F.; Deng, Y. Nano-Gold Catalysis in Fine Chemical Synthesis. *Chem. Rev.* **2012**, *112*, 2467–2505.
- (2) Stratakis, M.; Garcia, H. Catalysis by Supported Gold Nanoparticles: Beyond Aerobic Oxidative Processes. *Chem. Rev.* **2012**, *112*, 4469–4506.
- (3) Hashmi, A. S. K.; Hutchings, G. J. Gold Catalysis – the Journey Continues. *Catal. Sci. Technol.* **2013**, *3*, 2861.
- (4) Haruta, M. Gold as a Novel Catalyst in the 21st Century: Preparation, Working Mechanism and Applications. *Gold Bull.* **2004**, *37*, 27–36.
- (5) Della Pina, C.; Falletta, E. Gold-Catalyzed Oxidation in Organic Synthesis: A Promise Kept. *Catal. Sci. Technol.* **2011**, *1*, 1564–1571.
- (6) Mitsudome, T.; Kaneda, K. Gold Nanoparticle Catalysts for Selective Hydrogenations. *Green Chem.* **2013**, *15*, 2636–2654.
- (7) Corma, A.; Garcia, H. Supported Gold Nanoparticles as Catalysts for Organic Reactions. *Chem. Soc. Rev.* **2008**, *37*, 2096–2126.
- (8) Gladysz, J. A. Recoverable Catalysts. Ultimate Goals, Criteria of Evaluation, and the Green Chemistry Interface. *Pure Appl. Chem.* **2001**, *73*, 1319–1324.
- (9) Prati, L.; Villa, A. Gold Colloids: From Quasi-Homogeneous to Heterogeneous Catalytic Systems. *Acc. Chem. Res.* **2014**, *47*, 855–863.
- (10) Geukens, I.; De Vos, D. E. Organic Transformations on Metal Nanoparticles: Controlling Activity, Stability, and Recyclability by Support and Solvent Interactions. *Langmuir* **2013**, *29*, 3170–3178.

- (11) Wu, Y. Y.; Mashayekhi, N. A.; Kung, H. H. Au–metal Oxide Support Interface as Catalytic Active Sites. *Catal. Sci. Technol.* **2013**, *3*, 2881–2891.
- (12) Taguchi, A.; Schüth, F. Ordered Mesoporous Materials in Catalysis. *Microporous Mesoporous Mater.* **2005**, *77*, 1–45.
- (13) Zeng, H. C. Integrated Nanocatalysts. *Acc. Chem. Res.* **2013**, *46*, 226–235.
- (14) Huang, S.; Hara, K.; Fukuoka, A. Green Catalysis for Selective CO Oxidation in Hydrogen for Fuel Cell. *Energy Environ. Sci.* **2009**, *2*, 1060–1068.
- (15) Wen, C.; Zhu, Y.; Ye, Y.; Zhang, S.; Cheng, F.; Liu, Y.; Wang, P.; Tao, F. F. Water-Gas Shift Reaction on Metal Nanoclusters Encapsulated in Mesoporous Ceria Studied with Ambient-Pressure X-Ray Photoelectron Spectroscopy. *ACS Nano* **2012**, *6*, 9305–9313.
- (16) Luque, R.; García Martínez, J. From Mesoporous Supports to Mesoporous Catalysts: Introducing Functionality to Mesoporous Materials. *ChemCatChem* **2013**, *5*, 827–829.
- (17) Ren, Y.; Ma, Z.; Bruce, P. G. Ordered Mesoporous Metal Oxides: Synthesis and Applications. *Chem. Soc. Rev.* **2012**, *41*, 4909–4927.
- (18) Wang, S.; Zhao, Q.; Wei, H.; Wang, J.-Q.; Cho, M.; Cho, H. S.; Terasaki, O.; Wan, Y. Aggregation-Free Gold Nanoparticles in Ordered Mesoporous Carbons: Toward Highly Active and Stable Heterogeneous Catalysts. *J. Am. Chem. Soc.* **2013**, *135*, 11849–11860.
- (19) Corma, A.; González-Arellano, C.; Iglesias, M.; Sánchez, F. Gold Nanoparticles and gold(III) Complexes as General and Selective Hydrosilylation Catalysts. *Angew. Chem., Int. Ed.* **2007**, *46*, 7820–7822.
- (20) An, K.; Musselwhite, N.; Kennedy, G.; Pushkarev, V. V.; Baker, L. R.; Somorjai, G. a. Preparation of Mesoporous Oxides and Their Support Effects on Pt Nanoparticle Catalysts in Catalytic Hydrogenation of Furfural. *J. Colloid Interface Sci.* **2013**, *392*, 122–128.
- (21) Kwon, Y.; Lai, S. C. S.; Rodriguez, P.; Koper, M. T. M. Electrocatalytic Oxidation of Alcohols on Gold in Alkaline Media: Base or Gold Catalysis? *J. Am. Chem. Soc.* **2011**, *133*, 6914–6917.
- (22) Diao, P.; Zhang, D.; Guo, M.; Zhang, Q. Electrocatalytic Oxidation of CO on Supported Gold Nanoparticles and Submicroparticles: Support and Size Effects in Electrochemical Systems. *J. Catal.* **2007**, *250*, 247–253.
- (23) Sánchez, V. M.; Martínez, E. D.; Martínez Ricci, M. L.; Troiani, H.; Soler-Illia, G. J. A. A. Optical Properties of Au Nanoparticles Included in Mesoporous TiO<sub>2</sub> Thin Films: A Dual Experimental and Modeling Study. *J. Phys. Chem. C* **2013**, *117*, 7246–7259.
- (24) Fuertes, M. C.; Marchena, M.; Marchi, M. C.; Wolosiuk, A.; Soler-Illia, G. J. A. A. Controlled Deposition of Silver Nanoparticles in Mesoporous Single- or Multilayer Thin Films: From Tuned Pore Filling to Selective Spatial Location of Nanometric Objects. *Small* **2009**, *5*, 272–280.
- (25) Germain, P. S.; Pell, W. G.; Conway, B. E. Evaluation and Origins of the Difference between Double-Layer Capacitance Behaviour at Au-Metal and Oxidized Au Surfaces. *Electrochim. Acta* **2004**, *49*, 1775–1788.
- (26) Jiang, J.; Kucernak, A. Electrooxidation of Small Organic Molecules on Mesoporous Precious Metal Catalysts. *J. Electroanal. Chem.* **2003**, *543*, 187–199.
- (27) Viva, F. A.; Bruno, M. M.; Jobbágy, M.; Corti, H. R. Electrochemical Characterization of PtRu Nanoparticles Supported on Mesoporous Carbon for Methanol Electrooxidation. *J. Phys. Chem. C* **2012**, *116*, 4097–4104.
- (28) Wieckowski, A.; Chrzanoski, W. In *Interfacial Electrochemistry: Theory, Experiment, and Applications*; Wieckowski, A., Ed.; Marcel Dekker Inc.: New York, 1999; Chapter 51, pp 937–954.
- (29) Pan, Y.; Gao, Y.; Kong, D.; Wang, G.; Hou, J.; Hu, S.; Pan, H.; Zhu, J. Interaction of Au with Thin ZrO<sub>2</sub> Films: Influence of ZrO<sub>2</sub> Morphology on the Adsorption and Thermal Stability of Au Nanoparticles. *Langmuir* **2012**, *28*, 6045–6051.
- (30) Kašpar, J.; Fornasiero, P.; Hickey, N. Automotive Catalytic Converters: Current Status and Some Perspectives. *Catal. Today* **2003**, *77*, 419–449.
- (31) Wootsch, A.; Descorme, C.; Duprez, D. Preferential Oxidation of Carbon Monoxide in the Presence of Hydrogen (PROX) over Ceria–zirconia and Alumina-Supported Pt Catalysts. *J. Catal.* **2004**, *225*, 259–266.
- (32) Zelcer, A.; Soler-Illia, G. J. A. A. One-Step Preparation of UV Transparent Highly Ordered Mesoporous Zirconia Thin Films. *J. Mater. Chem. C* **2013**, *1*, 1359–1367.
- (33) Kosmulski, M. pH-Dependent Surface Charging and Points of Zero Charge. IV. Update and New Approach. *J. Colloid Interface Sci.* **2009**, *337*, 439–448.
- (34) Paul, A.; Mulholland, M.; Zaman, M. S. Ultraviolet Absorption of Cerium(III) and Cerium(IV) in Some Simple Glasses. *J. Mater. Sci.* **1976**, *11*, 2082–2086.
- (35) Cuenya, B. R. Synthesis and Catalytic Properties of Metal Nanoparticles: Size, Shape, Support, Composition, and Oxidation State Effects. *Thin Solid Films* **2010**, *518*, 3127–3150.
- (36) Karwacki, C. J.; Ganesh, P.; Kent, P. R. C.; Gordon, W. O.; Peterson, G. W.; Niu, J. J.; Gogotsi, Y. Structure–activity Relationship of Au/ZrO<sub>2</sub> Catalyst on Formation of Hydroxyl Groups and Its Influence on CO Oxidation. *J. Mater. Chem. A* **2013**, *1*, 6051–6062.
- (37) Hayden, B. E.; Pletcher, D.; Rendall, M. E.; Suchsland, J.-P. CO Oxidation on Gold in Acidic Environments: Particle Size and Substrate Effects. *J. Phys. Chem. C* **2007**, *111*, 17044–17051.
- (38) Vernoux, P.; Lizarraga, L.; Tsampas, M. N.; Sapountzi, F. M.; De Lucas-Consuegra, A.; Valverde, J.-L.; Souentie, S.; Vayenas, C. G.; Tsiplakides, D.; Balomenou, S.; Baranova, E. A. Ionically Conducting Ceramics as Active Catalyst Supports. *Chem. Rev.* **2013**, *113*, 8192–8260.
- (39) Wolosiuk, A.; Tognalli, N. G.; Martínez, E. D.; Granada, M.; Fuertes, M. C.; Troiani, H. E.; Bilmes, S. A.; Fainstein, A.; Soler-Illia, G. J. A. A. Silver Nanoparticle-Mesoporous Oxide Nanocomposite Thin Films: A Platform for Spatially Homogeneous SERS-Active Substrates with Enhanced Stability. *ACS Appl. Mater. Interfaces* **2014**, *6*, 5263–5272.
- (40) Rafti, M.; Brunsen, A.; Fuertes, M. C.; Azzaroni, O.; Soler-Illia, G. J. A. A. Heterogeneous Catalytic Activity of Platinum Nanoparticles Hosted in Mesoporous Silica Thin Films Modified with Polyelectrolyte Brushes. *ACS Appl. Mater. Interfaces* **2013**, *5*, 8833–8840.
- (41) Pushkarev, V. V.; Zhu, Z.; An, K.; Hervier, A.; Somorjai, G. A. Monodisperse Metal Nanoparticle Catalysts: Synthesis, Characterizations, and Molecular Studies Under Reaction Conditions. *Top. Catal.* **2012**, *55*, 1257–1275.
- (42) Fenger, R.; Fertitta, E.; Kirmse, H.; Thünemann, A. F.; Rademann, K. Size Dependent Catalysis with CTAB-Stabilized Gold Nanoparticles. *Phys. Chem. Chem. Phys.* **2012**, *14*, 9343–9349 The kinetic constants reported in this article have been normalized by the amount of gold to compare them with those reported in the present work.
- (43) Wunder, S.; Polzer, F.; Lu, Y.; Mei, Y.; Ballauff, M. Kinetic Analysis of Catalytic Reduction of 4-Nitrophenol by Metallic Nanoparticles Immobilized in Spherical Polyelectrolyte Brushes. *J. Phys. Chem. C* **2010**, *114*, 8814–8820.
- (44) Pradhan, N.; Pal, A.; Pal, T. Silver Nanoparticle Catalyzed Reduction of Aromatic Nitro Compounds. *Colloids Surf., A* **2002**, *196*, 247–257.
- (45) Nigra, M. M.; Ha, J.-M.; Katz, A. Identification of Site Requirements for Reduction of 4-Nitrophenol Using Gold Nanoparticle Catalysts. *Catal. Sci. Technol.* **2013**, *3*, 2976–2983.
- (46) Mahmoud, M. A.; Garlyyyev, B.; El-Sayed, M. A. Determining the Mechanism of Solution Metallic Nanocatalysis with Solid and Hollow Nanoparticles: Homogeneous or Heterogeneous. *J. Phys. Chem. C* **2013**, *117*, 21886–21893.
- (47) Mitra, A.; Jana, D.; De, G. A Facile Synthesis of Cubic (Im3m) Alumina Films on Glass with Potential Catalytic Activity. *Chem. Commun.* **2012**, *48*, 3333–3335.
- (48) Jin, Z.; Xiao, M.; Bao, Z.; Wang, P.; Wang, J. A General Approach to Mesoporous Metal Oxide Microspheres Loaded with Noble Metal Nanoparticles. *Angew. Chem., Int. Ed.* **2012**, *51*, 6406–6410.

(49) Ide, M. S.; Davis, R. J. The Important Role of Hydroxyl on Oxidation Catalysis by Gold Nanoparticles. *Acc. Chem. Res.* **2014**, *47*, 825–833.

(50) Calvo, A.; Yameen, B.; Williams, F. J.; Azzaroni, O.; Soler-Illia, G. J. A. Facile Molecular Design of Hybrid Functional Assemblies with Controllable Transport Properties: Mesoporous Films Meet Polyelectrolyte Brushes. *Chem. Commun.* **2009**, 2553–2555.

(51) Jaramillo, T. F.; Baeck, S.-H.; Cuenya, B. R.; McFarland, E. W. Catalytic Activity of Supported Au Nanoparticles Deposited from Block Copolymer Micelles. *J. Am. Chem. Soc.* **2003**, *125*, 7148–7149.

(52) Nagaraju, D. H.; Lakshminarayanan, V. Electrochemically Grown Mesoporous Gold Film as High Surface Area Material for Electro-Oxidation of Alcohol in Alkaline Medium. *J. Phys. Chem. C* **2009**, *113*, 14922–14926.

(53) Lima, R. B.; Varela, H. Catalytic Oxidation of Ethanol on Gold Electrode in Alkaline Media. *Gold Bull.* **2008**, *41*, 15–22.

(54) Jena, B. K.; Raj, C. R. Synthesis of Flower-like Gold Nanoparticles and Their Electrocatalytic Activity towards the Oxidation of Methanol and the Reduction of Oxygen. *Langmuir* **2007**, *23*, 4064–4070.